Target Detection in Hyperspectral Imagery via Sparse and Dense Hybrid Representation

Tan Guo, Fulin Luo, Lei Zhang, *Senior Member, IEEE*, Xiaoheng Tan, Juhua Liu, and Xiaocheng Zhou

***Abstract*— Representation-based target detectors for hyperspectral imagery (HSI) have recently aroused a lot of interests. However, existing methods ignore the dictionary structure and cannot guarantee an informative and discriminative representation of test pixels for target detection. To alleviate the problem, this letter proposes a novel sparse and dense hybrid representation-based target detector (SDRD). The proposed detector adopts the idea that the relationship between the background and the target sub-dictionaries is a collaborative competition. The structure of the dictionary is discovered and preserved by learning a sparse and dense hybrid representation for test pixel. Benefitting from this, a compact and discriminative representation can be obtained to better represent the test pixel for an improved detection performance. Experimental results on several HSI data sets verify the effectiveness of SDRD in comparison with several state-of-the-art methods.**

***Index Terms*— Dense representation, dictionary structure, hyperspectral imagery (HSI), sparse representation, target detection.**

Manuscript received April 8, 2019; revised May 24, 2019; accepted July 2, 2019. This work was supported in part by the National Natural Science Foundation of China under Grant 61801336, Grant 61771079, Grant 61571069, Grant 61601335, and Grant 61801072, in part by the Science and Technology Research Program of the Chongqing Municipal Education Commission under Grant KJQN201800632 and Grant KJQN201800617, in part by the Chongqing Science and Technology Commission under Grant cstc2018jcyjAX0344, Grant cstc2018jcyjAX0549, and Grant cstc2017zdcy-zdzxX0002, in part by the Open Research Fund of Key Laboratory of Digital Earth Science, Institute of Remote Sensing and Digital Earth, Chinese Academy of Sciences, under Grant 2017LDE002, in part by the Open Research Fund of Hubei Key Laboratory of Applied Mathematics, Hubei University, under Grant HBAM201803, in part by the Open Research Fund of Key Laboratory of Spatial Data Mining and Information Sharing of Ministry of Education, Fuzhou University, under Grant 2019LSDMIS06, and in part by the Special Project on the Industrial Technology Innovation of Suzhou under Grant SYG201714. *(Corresponding author: Fulin Luo.)*

T. Guo is with the School of Communication and Information Engineering, Chongqing University of Posts and Telecommunications, Chongqing 400065, China (e-mail: guot@cqupt.edu.cn).

F. Luo is with the State Key Laboratory of Information Engineering in Surveying, Mapping and Remote Sensing, Wuhan University, Wuhan 430079, China, and also with the Hubei Key Laboratory of Applied Mathematics, Faculty of Mathematics and Statistics, Hubei University, Wuhan 430062, China (e-mail: luoflyn@163.com).

L. Zhang and X. Tan are with the School of Microelectronics and Communication Engineering, Chongqing University, Chongqing 400044, China (e-mail: leizhang@cqu.edu.cn; txh@cqu.edu.cn).

J. Liu is with the School of Printing and Packaging, Wuhan University, Wuhan 430079, China, and also with the Suzhou Institute, Wuhan University, Suzhou 215123, China (e-mail: liujuhua@whu.edu.cn).

X. Zhou is with the Key Laboratory of Spatial Data Mining and Information Sharing of Ministry of Education, Fuzhou University, Fuzhou 350116, China (e-mail: zhouxc@fzu.edu.cn).

Color versions of one or more of the figures in this letter are available online at http://ieeexplore.ieee.org.

Digital Object Identifier 10.1109/LGRS.2019.2927256

I. Introduction

HYPERSPECTRAL imagery (HSI) contains hundreds of narrow contiguous spectral bands, and each pixel can form a continuous spectrum [1], [2]. HSI can be used to discriminate different materials since they differently reflect electromagnetic energy at specific wavelengths [3]–[6]. Target detection aims to separate the specific target pixels from various backgrounds with the known target spectra properties, which can be viewed as a two-class classification problem. In hyperspectral target detection, pixels are labeled as target or background based on their spectral characteristics [7]. The technique has attracted significant interests in HSI to detect the targets for rare minerals, oil pollution, and man-made objects.

In view of its wide application, extensive efforts have been devoted to solving the hyperspectral target detection problem. Traditional target detection algorithms are usually based on statistic hypothesis, such as constrained energy minimization (CEM) [8], adaptive coherence/cosine estimator (ACE) [9], and the spectral matched filter (SMF) [10]. However, the statistics-based methods usually follow certain assumptions, which are not always satisfied in reality. Recently, sparsity-based techniques have been developed for many signal processing and HSI applications [4], [5], [11]–[21], such as classification [4], [5], unmixing [11], and target detection [16]–[21]. Motivated by the fact that the test pixels can be represented by a few training atoms from both the target and background sub-dictionaries, and the recovered representations can be obtained by solving a sparsity-constrained optimization problem, Chen *et al.* [16] proposed a sparse representation-based model for hyperspectral target detection. They further proposed a joint sparse representation-based detector using surrounding pixels to jointly represent the center pixel [17]. Zhang *et al.* [19] united the sparse representation and binary hypothesis and developed a sparse representation-based binary hypothesis (SRBBH) model. Recently, a binary-class collaborative representation-based detector has been proposed using collaborative representation and background purification [21]. An important advantage of these approaches is that no explicit assumptions are needed for the statistical distribution characteristics of data.

In sparsity-based target detectors, a test pixel is transformed into the background subspace or the target and background subspace and sparsely represented as a linear combination of a few elements from a spectral dictionary that contains the target and background spectra. However, samples in dictionaries are always limited, which may not provide enough

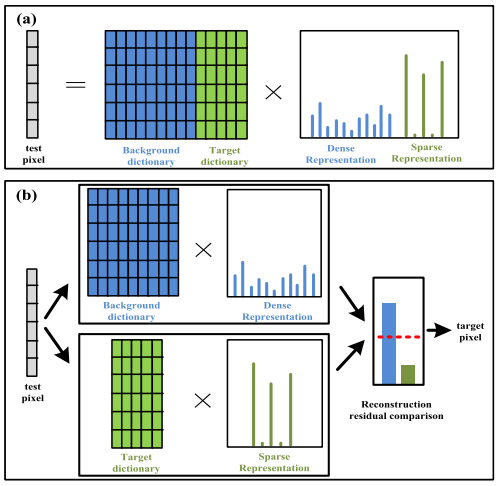

Fig. 1. Overview of the proposed SDRD. (a) Sparse representation and a dense representation are jointly learned on the background and the target sub-dictionaries for the test pixel. (b) Afterward, the decision is made by the comparison of the reconstruction residual from the two sub-dictionaries.

expressive power for the test pixel. Existing approaches cannot make full use of the dictionary structure, namely, the background and the target sub-dictionaries should make different contributions in representing the test pixel. To consider the dictionary structure, we propose to simultaneously learn a sparse representation on the target dictionary and a dense representation on the background dictionary and construct a novel detector termed sparse and dense hybrid representation-based detector (SDRD), as shown in Fig. 1. Specifically, a dense representation on background dictionary is used to provide adequate expressive ability, and a sparse representation on the target dictionary can enhance the discriminant performance. With this mechanism, the target dictionary and the background dictionary will compete with each other to win their representation share of the test pixel, which will make the obtained representation more discriminative and informative for target detection.

The rest of this letter is structured as follows. Section II describes the proposed detector in detail. Section III shows the experimental effectiveness of the proposed detector. Conclusions are drawn in Section IV.

II. Hyperspectral Target Detection via Sparse and Dense Hybrid Representation

A. Sparse and Dense Hybrid Representation-Based Detector

Consider hyperspectral data $\mathbf{X} = [\mathbf{X}_t; \mathbf{X}_b]$, where target samples $\mathbf{X}_t = \{x_i\}_{i=1}^{N_t} \in \mathbb{R}^d$ (d is the number of spectral bands) and N_t is the total number of target samples. Background samples $\mathbf{X}_b = \{\mathbf{x}_i\}_{i=1}^{N_b} \in \mathbb{R}^d$ and N_b is the number of background samples. The key idea of the proposed SDRD is to jointly learn a sparse representation $\boldsymbol{\alpha}_b$ on the background dictionary $\mathbf{X}_b$ and a dense representation $\boldsymbol{\alpha}_t$ on the target dictionary $\mathbf{X}_t$ for a test pixel $\mathbf{y}$ as follows:

$$\begin{aligned} &\min_{\boldsymbol{\alpha}_b, \boldsymbol{\alpha}_t, \boldsymbol{e}} \ \|\boldsymbol{\alpha}_b\|_1 + \gamma \|\boldsymbol{\alpha}_t\|_2^2 + \beta \|\boldsymbol{e}\|_2^2 \\ &\text{s.t. } \mathbf{y} = \mathbf{X}_b\boldsymbol{\alpha}_b + \mathbf{X}_t\boldsymbol{\alpha}_t + \boldsymbol{e}. \end{aligned} \tag{1}$$

From the perspective of modeling, $\|\cdot\|_1$ will promote a sparse representation $\boldsymbol{\alpha}_b$, while $\|\cdot\|_2^2$ encourages a dense representation $\boldsymbol{\alpha}_t$. The term $\|\boldsymbol{e}\|_2^2$ is used to model dense noise in data. This model can be optimized by the augmented Lagrange multiplier (ALM) scheme [22]. Specifically, the augmented Lagrangian function for (1) is

$$\begin{aligned} \mathcal{L}(\boldsymbol{\alpha}_b, \boldsymbol{\alpha}_b, \boldsymbol{e}, \boldsymbol{\theta}) = \|\boldsymbol{\alpha}_b\|_1 + \gamma \|\boldsymbol{\alpha}_t\|_2^2 + \beta\|\boldsymbol{e}\|_2^2 \\ + \frac{\mu}{2}\|\mathbf{y} - \mathbf{X}_b\boldsymbol{\alpha}_b - \mathbf{X}_t\boldsymbol{\alpha}_t - \boldsymbol{e} + \boldsymbol{\theta}/\mu\|_2^2 \end{aligned} \tag{2}$$

where $\boldsymbol{\theta}$ is the Lagrange multipliers and $\mu > 0$ is a penalty parameter. The augmented Lagrangian is minimized along one coordinate direction at each iteration, i.e., minimizing the loss with respect to one variable with the other variables fixed. The detailed iteration optimization procedures are as follows:

Updating $\boldsymbol{e}$: update $\boldsymbol{e}$ by setting the derivative $(\partial\mathcal{L}/\partial e) = 0$

$$\boldsymbol{e} = (\mu/2\beta + 1)(\mathbf{y} - \mathbf{X}_b\boldsymbol{\alpha}_b - \mathbf{X}_t\boldsymbol{\alpha}_t + \boldsymbol{\theta}/\mu). \tag{3}$$

Updating $\boldsymbol{\alpha}_b$: update $\boldsymbol{\alpha}_b$ by solving the following l_1-norm minimization problem:

$$\boldsymbol{\alpha}_b = \underset{\alpha_b}{\operatorname{argmin}} \|\boldsymbol{\alpha}_b\|_1 + \frac{\mu}{2}\|\mathbf{X}_b\boldsymbol{\alpha}_b - (\mathbf{y} - \mathbf{X}_t\boldsymbol{\alpha}_t + \boldsymbol{\theta}/\mu)\|_2^2 \tag{4}$$

which can be solved as an l_1-minimization problem.

Updating $\boldsymbol{\alpha}_t$: update $\boldsymbol{\alpha}_t$ by setting the derivative with respect to $\boldsymbol{\alpha}_t$ as zero, i.e., $(\partial\mathcal{L}/(\partial\boldsymbol{\alpha}_t)) = 0$

$$\boldsymbol{\alpha}_t = \mu\left(2\gamma\,\mathbf{I} + \mu\mathbf{X}_t^{\mathrm{T}}\mathbf{X}_t\right)^{-1}\mathbf{X}_t^{\mathrm{T}}(\mathbf{y} - \mathbf{X}_b\boldsymbol{\alpha}_b - \boldsymbol{e} + \boldsymbol{\theta}/\mu). \tag{5}$$

Then, the multipliers and penalty parameter can be adjusted as follows:

$$\begin{cases} \boldsymbol{\theta} = \boldsymbol{\theta} + \mu(\mathbf{y} - \mathbf{X}_b\boldsymbol{\alpha}_b - \mathbf{X}_t\boldsymbol{\alpha}_t - \mathbf{e}) \\ \mu = \min(\rho\mu, \mu_{\max}). \end{cases} \tag{6}$$

Repeat the above steps until the following convergence condition is reached:

$$\|\mathbf{y} - \mathbf{X}_b\boldsymbol{\alpha}_b - \mathbf{X}_t\boldsymbol{\alpha}_t - \boldsymbol{e}\|_2^2 < \epsilon. \tag{7}$$

With the above procedures, the obtained optimal $\boldsymbol{\alpha}_b$ and $\boldsymbol{\alpha}_t$ are compact and discriminative for target detection. The test pixel can be reconstructed by $\widehat{\mathbf{y}}_b = \mathbf{X}_b\boldsymbol{\alpha}_b$ and $\widehat{\mathbf{y}}_t = \mathbf{X}_t\boldsymbol{\alpha}_t$. The reconstructed spectrum can be determined by comparing the reconstruction residual of the mean squared error as follows:

$$r_0(\mathbf{y}) = \|\mathbf{y} - \widehat{\mathbf{y}}_b\|_2 \tag{8}$$

$$r_1(\mathbf{y}) = \|\mathbf{y} - \widehat{\mathbf{y}}_t\|_2. \tag{9}$$

The label of the test pixel is determined by these residuals, and the decision is made as

$$\text{label}(\mathbf{y}) = \varphi(r_1(\mathbf{y}) - r_0(\mathbf{y})) \tag{10}$$

where

$$\varphi(x) = \begin{cases} 1, & x > \delta \\ 0, & x \le \delta \end{cases}$$

is a classification function with a predefined threshold δ. Algorithm 1 shows the procedure of SDRD.

Algorithm 1 Procedure for SDRD

Input: $\mathbf{X}_b$,$\mathbf{X}_t$, β,γ , and δ.

1. Initialize:

$$\boldsymbol{\alpha}_b = \mathbf{0}, \boldsymbol{\alpha}_t = \mathbf{0}, \boldsymbol{e} = \mathbf{0}, \boldsymbol{\theta} = 0, \mu{=}1, \mu_{max}{=}10^6, \rho = 1.1, \epsilon = 10^{-6}.$$

2. **While** *not converged* **do**
   3. Update $\boldsymbol{e}$ by (3).
   4. Update $\boldsymbol{\alpha}_b$ by (4).
   5. Update $\boldsymbol{\alpha}_t$ by (5).
   6. Update the multipliers and penalty parameter by (6).
   7. Check the convergence condition by (7).
8. **End while**
9. Calculate the reconstruction from sub-dictionaries as in (8) and (9).
10. Make decision via (10).

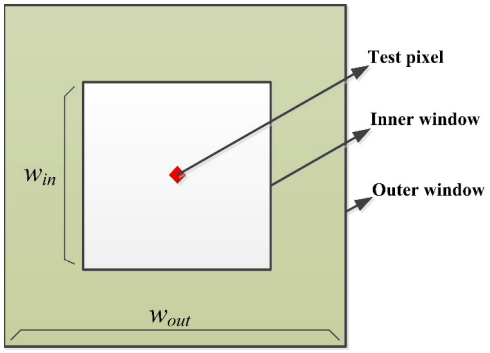

Fig. 2. Illustration of the dual window to construct the background dictionary. In this letter, the target dictionary is assumed to be known and a sliding dual-window strategy is used to obtain the background dictionary adaptively.

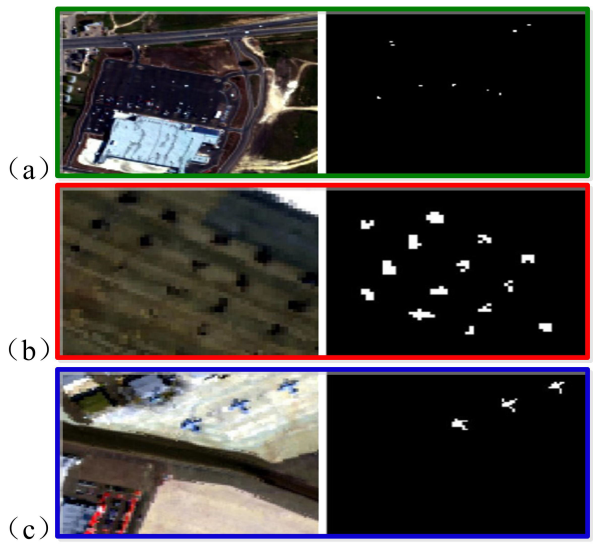

Fig. 3. (Left) Hyperspectral image scene. (Right) Ground truth. (a) HYDICE. (b) AVIRIS I. (c) AVIRIS II.

TABLE I
PARAMETER SETTINGS FOR DIFFERENT DETECTORS IN THE EXPERIMENTS

Detectors	Parameters (<:, :> means < w_{out}, w_{in} >)
ACE	<13,5> for HYDICE, AVIRIS I; <17,7> for AVIRIS II.
SMF	<13,5> for HYDICE, AVIRIS I; <17,7> for AVIRIS II.
STD	<13,5> for HYDICE, AVIRIS I; <17,7> for AVIRIS II; sparsity level: 4 for AVIRIS, 10 for HYDICE.
SRBBH	<13,5> for HYDICE, AVIRIS I; <17,7> for AVIRIS II; sparsity level: 10.
SDRD	<13,5> for HYDICE, AVIRIS I; <17,7> for AVIRIS II; $\gamma = \beta = 12$.

B. Background and Target Dictionary Construction

Dictionaries for target and background can be designed using the given training samples. However, there is usually a lack of training data, especially for the target class. In this letter, we use one spectral signature for each type of target to construct the target library. While the background dictionary is generated locally for each test pixel using a dual window centered at the pixel of interest. For each test pixel $\mathbf{y}$, surrounding data are collected inside the outer window with size $w_{\text{out}} \times w_{\text{out}}$ and outside the inner window with size $w_{\text{in}} \times w_{\text{in}}$, as shown in Fig. 2. The pixels in the region between the inner window and the outer window form the background dictionary.

III. EXPERIMENT EVALUATIONS

To evaluate the performance of the proposed detector, some real HSIs were tested in the experiments. SDRD was compared with some representative methods, such as ACE [9], SMF [10], sparse representation-based target detection (STD) [16], and SRBBH [19]. For all the detectors, we use the same given target spectrum as the input priori target spectrum. For the detectors ACE and SMF, we use the pixels in the dual-window to construct the background covariance matrix. For STD and SRBBH, the pixels in the dual-window are used to construct the background dictionary. Two airborne visible/infrared imaging spectrometer (AVIRIS) data sets [21] and the hyperspectral digital imagery collection experiment (HYDICE) data set [20] are used in the experiments, as shown in Fig. 3. As suggested by the original papers, the detailed parameter settings for different detectors are shown in Table I.

A. HYDICE Data Set

The first data set was collected by the HYDICE sensor with a spatial resolution of 2 m and 210 spectral bands. After removing the low SNR, water absorption, and bad bands (1–4, 76, 87, 101–111, 136–153, and 198–210), 162 bands remained. The HYDICE data set and its ground-truth information is shown in Fig. 3(a), which has 150 × 150 pixels, and the vehicles were selected as the targets to detect, which has 21 pixels. We used the receiver operating characteristic (ROC) curves to evaluate the experimental results of different methods. The ROC curve is shown in Fig. 4.

B. AVIRIS Data Set

The second and third data sets are collected by the AVIRIS from San Diego with a spatial resolution of 3.5 m. After removing the low SNR, water absorption, and bad

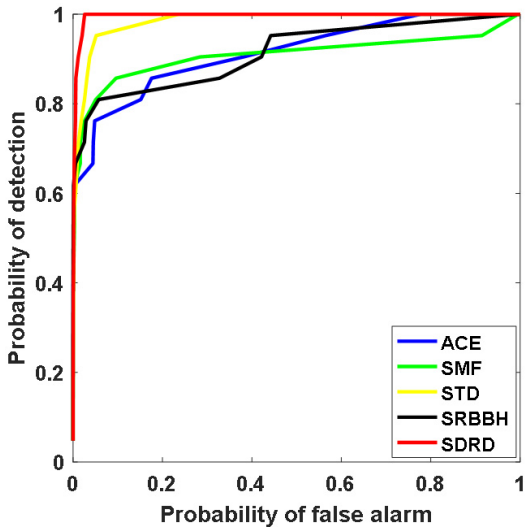

Fig. 4. ROC performance of different detectors on HYDICE.

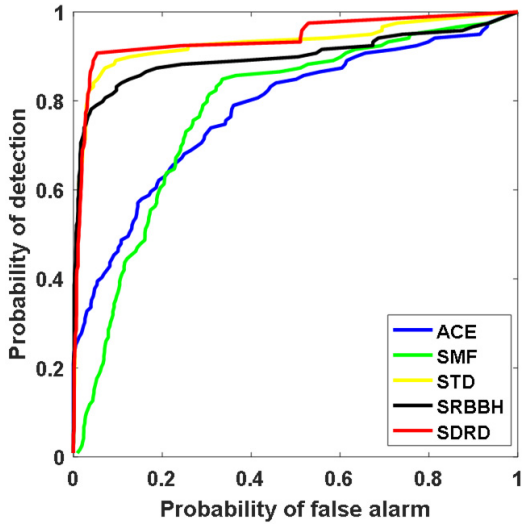

Fig. 5. ROC performance of different detectors on AVIRIS I.

bands (1–6, 33–35, 97, 107–113, 153–166, and 221–224), 189 bands remained. The AVIRIS I data set and AVIRIS II data set and their ground-truth information are shown in Fig. 3(b) and (c), which have 60 × 60 pixels and 100 × 100 pixels, respectively. For the AVIRIS I data set, there are 14 airplanes containing 119 pixels to detect. For the AVIRIS II data set, the airplanes were selected as the targets to detect, which has 58 pixels. Similarly, we used the ROC curves to evaluate the experimental results of different methods. The ROC curves are shown in Figs. 5 and 6.

More specifically, the area under the curve (AUC) values of different detectors for the three data sets are shown in Table II.

In addition, we provide the separation diagrams between the target and the background on the three data sets to show the separation ability of different detectors, as shown in Figs. 7–9.

By analysis and comparison, the traditional methods, such as ACE and SMF, do not perform very well, because these methods require data satisfying strict assumptions for

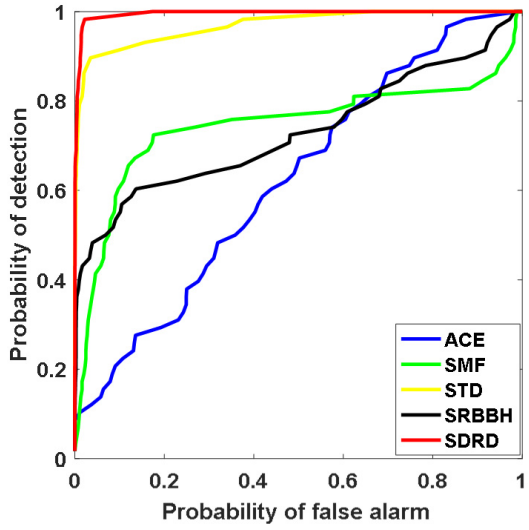

Fig. 6. ROC performance of different detectors on AVIRIS II.

TABLE II
AUC VALUES OF DIFFERENT DETECTORS FOR THE THREE DATA SETS

Detectors	Datasets		
	HYDICE	AVIRIS I	AVIRIS II
ACE [9]	0.9140	0.7799	0.6219
SMF [10]	0.9087	0.7769	0.7439
STD [16]	0.9848	0.9303	0.9695
SRBBH [19]	0.9138	0.8989	0.7293
SDRD	0.9962	0.9409	0.9956

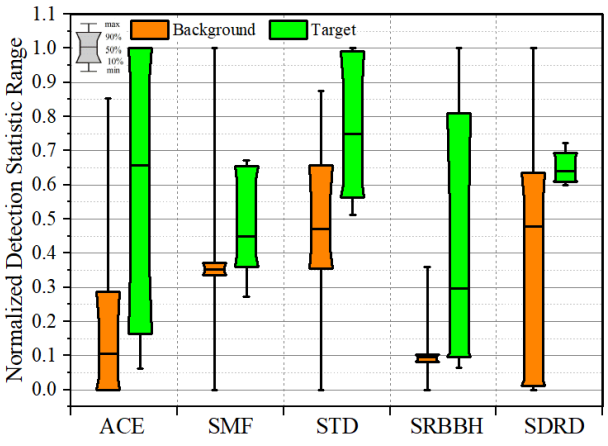

Fig. 7. Separability map of all detectors for HYDICE data set.

application, while data is difficult to match the assumption generally. Unlike traditional methods, representation learning-based detectors do not assume any statistical distribution characteristics of the observed data and achieve promising performance. These methods use the data reconstruction concept to find an informative representation of the test pixel to guide the following target detection. Nevertheless, a naïve uni-structure representation cannot reveal the underlying structure of the dictionary well, which will restrict their performance. Comparatively speaking, the proposed detector can achieve better performance and higher AUC values under considered

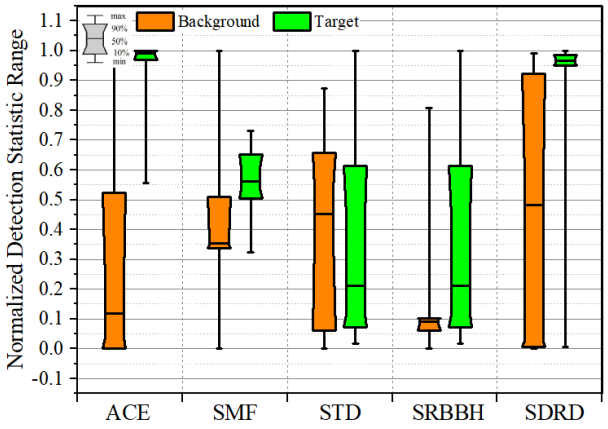

Fig. 8. Separability map of all detectors for AVIRIS I data set.

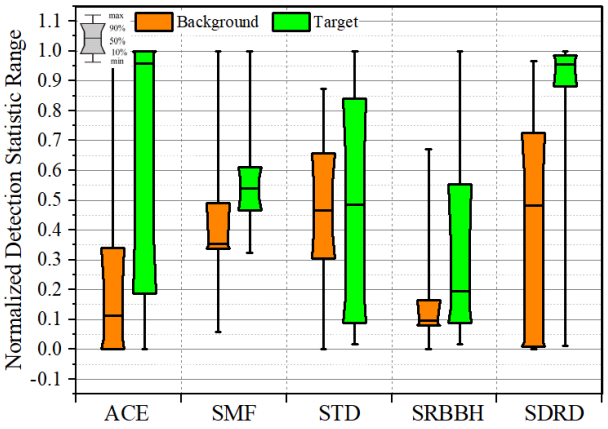

Fig. 9. Separability map of all detectors for AVIRIS II data set.

target detection tasks. In addition, the separation diagrams further show that the developed SDRD can efficiently distinguish targets from a background in general. The benefits can be attributed to the full utilization of the dictionary structure, which is discovered and preserved by learning a sparse and dense hybrid representation. The distinguishing property of sparse representation will boost the discriminant performance of the target dictionary atoms for the test pixel, while the collaborative property of dense representation will promote better representation of the test pixel. The collaborative and competitive representations on the background and the target sub-dictionaries can improve the final target detection performance as verified by the above experimental results.

IV. Conclusion

This letter aims to fully reveal the structure of the dictionary by learning a structural representation for target detection in HSI. To this end, we propose to learn a sparse and dense hybrid representation via joint optimization, resulting in a novel SDRD. In SDRD, the background and the target sub-dictionaries are assumed to competitively and collaboratively represent the test pixel. Thus, a compact and discriminative representation can be achieved for better representation of the test pixel. Then, the final decision is made by comparing the reconstruction residuals on the background and the target sub-dictionaries. Experimental results show that the proposed method can yield promising detection performance.

References

[1] D. Manolakis and G. Shaw, "Detection algorithms for hyperspectral imaging applications," *IEEE Signal Process. Mag.*, vol. 19, no. 1, pp. 29–43, Jan. 2002.

[2] B. Du, Y. Zhang, L. Zhang, and D. Tao, "Beyond the sparsity-based target detector: A hybrid sparsity and statistics-based detector for hyperspectral images," *IEEE Trans. Image Process.*, vol. 25, no. 11, pp. 5345–5357, Nov. 2016.

[3] X. Lu, W. Zhang, and X. Li, "A hybrid sparsity and distance-based discrimination detector for hyperspectral images," *IEEE Trans. Geosci. Remote Sens.*, vol. 56, no. 3, pp. 1704–1717, Mar. 2018.

[4] F. Luo, B. Du, L. Zhang, L. Zhang, and D. Tao, "Feature learning using spatial-spectral hypergraph discriminant analysis for hyperspectral image," *IEEE Trans. Cybern.*, vol. 49, no. 7, pp. 2406–2419, Jul. 2019.

[5] F. Luo, H. Huang, Y. Duan, J. Liu, and Y. Liao, "Local geometric structure feature for dimensionality reduction of hyperspectral imagery," *Remote Sens.*, vol. 9, no. 8, p. 790, Aug. 2017.

[6] T. Lei, Y. Zhang, Z. Lv, S. Li, S. Liu, and A. K. Nandi, "Landslide inventory mapping from bitemporal images using deep convolutional neural networks," *IEEE Geosci. Remote Sens. Lett.*, vol. 16, no. 6, pp. 982–986, Jun. 2019. doi: 10.1109/LGRS.2018.2889307.

[7] D. Manolakis, E. Truslow, M. Pieper, T. Cooley, and M. Brueggeman, "Detection algorithms in hyperspectral imaging systems: An overview of practical algorithms," *IEEE Signal Process. Mag.*, vol. 31, no. 1, pp. 24–33, Jan. 2014.

[8] Q. Du, H. Ren, and C. I. Chang, "A comparative study for orthogonal subspace projection and constrained energy minimization," *IEEE Trans. Geosci. Remote Sens.*, vol. 41, no. 6, pp. 1525–1529, Jun. 2003.

[9] D. Manolakis, D. Marden, and G. A. Shaw, "Hyperspectral image processing for automatic target detection applications," *Lincoln Lab. J.*, vol. 14, no. 1, pp. 79–116, Jan. 2003.

[10] N. M. Nasrabadi, "Regularized spectral matched filter for target recognition in hyperspectral imagery," *IEEE Signal Process. Lett.*, vol. 15, pp. 317–320, 2008.

[11] X. Wang, Y. Zhong, L. Zhang, and Y. Xu, "Spatial group sparsity regularized nonnegative matrix factorization for hyperspectral unmixing," *IEEE Trans. Geosci. Remote Sens.*, vol. 55, no. 11, pp. 6287–6304, Nov. 2017.

[12] J. Gui, Z. Sun, W. Jia, R. Hu, Y. Lei, and S. Ji, "Discriminant sparse neighborhood preserving embedding for face recognition," *Pattern Recognit.*, vol. 45, no. 8, pp. 2884–2893, Aug. 2012.

[13] J. Gui, D. Tao, Z. Sun, Y. Luo, X. You, and Y. Y. Tang, "Group sparse multiview patch alignment framework with view consistency for image classification," *IEEE Trans. Image Process.*, vol. 23, no. 7, pp. 3126–3137, Jul. 2014.

[14] T. Guo, L. Zhang, X. Tan, L. Yang, and Z. Lianga, "Data induced masking representation learning for face data analysis," *Knowl.-Based Syst.*, vol. 177, pp. 82–93, Aug. 2019.

[15] J. Gui, Z. Sun, S. Ji, D. Tao, and T. Tan, "Feature selection based on structured sparsity: A comprehensive study," *IEEE Trans. Neural Netw. Learn. Syst.*, vol. 28, no. 7, pp. 1490–1507, Jul. 2017.

[16] Y. Chen, N. M. Nasrabadi, and T. D. Tran, "Sparse representation for target detection in hyperspectral imagery," *IEEE J. Sel. Topics Signal Process.*, vol. 5, no. 3, pp. 629–640, Jun. 2011.

[17] Y. Chen, N. M. Nasrabadi, and T. D. Tran, "Simultaneous joint sparsity model for target detection in hyperspectral imagery," *IEEE Geosci. Remote Sens. Lett.*, vol. 8, no. 4, pp. 676–680, Jul. 2011.

[18] Y. Zhang, B. Du, and L. Zhang, "Regularization framework for target detection in hyperspectral imagery," *IEEE Geosci. Remote Sens. Lett.*, vol. 11, no. 1, pp. 313–317, Jan. 2014.

[19] Y. Zhang, B. Du, and L. Zhang, "A sparse representation-based binary hypothesis model for target detection in hyperspectral images," *IEEE Trans. Geosci. Remote Sens.*, vol. 53, no. 3, pp. 1346–1354, Mar. 2015.

[20] W. Li, Q. Du, and B. Zhang, "Combined sparse and collaborative representation for hyperspectral target detection," *Pattern Recognit.*, vol. 48, no. 12, pp. 3904–3916, Dec. 2015.

[21] D. Zhu, B. Du, and L. Zhang, "Binary-class collaborative representation for target detection in hyperspectral images," *IEEE Geosci. Remote Sens. Lett.*, vol. 16, no. 7, pp. 1100–1104, Jul. 2019. doi: 10.1109/LGRS.2019.2893395.

[22] D. P. Bertsekas, *Constrained Optimization and Lagrange Multiplier Methods*. New York, NY, USA: Academic, 1996.